Impact resistance of six-strut tensegrity

Zhaojun Liu, Xian Xu*, Meijia Wang, Ruhe Mei

Space Structures Research Center, College of Civil Engineering and Architecture, Zhejiang University, 866 Yuhangtang Road, Hangzhou, Zhejiang 310058, China
Key Laboratory for Space Structures of Zhejiang Province , 866 Yuhangtang Road, Hangzhou, Zhejiang 310058, China
Innovatgion Center of Yangtze River Delta, Zhejiang University, 828 Zhongxing Road, Jiashan County, Jiaxing, Zhejiang 314100, China
xianxu@zju.edu.cn

Abstract

Tensegrity is a special structural system consisting of struts and tendons. The system possesses remarkable deformability, rendering it suitable as a foundational framework for soft robots. The impact resistance of tensegrity-based robots is a critical property when they are used in extraterrestrial and disaster rescue scenarios. In this paper, a dynamic model of a six-strut tensegrity with a center payload is developed and the finite element method is used to simulate the dynamic behavior of the tensegrity free-falling from a given height to a rigid ground. The center payload of the system is assumed to be contained by a cubic box which is connected to the tensegrity by 24 tendons. To ensure the safety of the system, it is required that all the structural components including the tendons, struts, and the cubic box do not yield or buckle. Various properties of members, such as stiffness of tendons, prestress, cross-sectional area, length and material of struts, are examined to assess their influence on the maximum allowable free-falling height achievable by the six-strut tensegrity. It is found that using struts with high stiffness-to-density ratio and tendons with high stiffness can enhance the impact resistance. Furthermore, it is observed that, within a specific range, increasing the size of the tensegrity can enhance its impact resistance.

Keywords: six-strut tensegrity, impact resistance, finite element, dynamic analysis, parametric study

1. Introduction

The word 'Tensegrity' is used to describe a special structural system consisting of compression elements (struts) and tension elements (tendons)[1]. By definition, all the one-dimensional structural members of the system are axially loaded[2]. Thus, the shape of the tensegrity system is closely related to the prestress in the members. This unique property gives it many advantages such as scalability, high payload-to-mass ratio, and robustness[3], which renders it suitable as a skeleton of some engineering platforms, such as smart structures[4], deployable structures[5], and robots[6].

Much attention has been paid to tensegrity robots due to their remarkable deformability and efficiency recently. Many researchers focus on locomoting control of tensegrity robots for the exploration of extraterrestrial and disaster rescue scenarios. For example, Paul et al. designed a three-strut tensegrity robot that realized crawling gaits by using servomotors to drive tendons[7]. In [8], a small tensegrity robot that moved simply by using motors to vibrate it at specific frequencies was designed. NASA and the Agogino team proposed several types of spherical tensegrity robots to achieve rolling motions by driving tendons[9]-[12]. Zheng et al. presented a strut-actuated tensegrity robot to realize rolling motion[13].

Tensegrity robots have the ability to distribute forces in the members globally by changing systems' shape when they are subjected to unexpected impact forces. This feature makes them well-suited for a robust platform to explore complex environments, such as extraterrestrial11 and disaster rescue12 scenarios. Then, some researchers began to pay attention to the response of the tensegrity system during the landing impact. Rimoli used a discrete model to perform virtual drop tests on a tensegrity planetary lander considering the post-buckling behavior of tensegrity members[14], [15]. Zhang performed lots of drop experiments of the tensegrity lander prototypes to study the effect on the acceleration of payload under different designs of prototypes[16]. Wang et al. investigated the dynamic behavior of a DHT tensegrity lander during impact, using the finite element method for nonlinear tensegrity dynamics and ground dynamics[17]. However, these studies focus more on the effect of structural parameters on the maximum acceleration of the payload due to the work scene of the system, and the collision between struts and payload was not considered due to the payload was simplified as a node with mass. In this study, according to the failure criteria of the structural components, various properties of members are examined to assess their influence on the maximum allowable free-falling height achievable by the six-strut tensegrity.

This paper is organized as follows. Section 2 describes a dynamic model of a six-strut tensegrity with a center payload and introduces the simulation of the dynamic behavior of the tensegrity free-falling from a given height to a rigid ground. Section 3 gives simulation results of the tensegrity dynamics behavior with different tendons stiffness, prestress, struts cross-sectional area, struts length, and struts material. At last, Section 4 concludes the paper.

2. Modelling of a six-strut tensegrity with a center payload

2.1. Control equation on tensegrity dynamic
The control equation on tensegrity dynamic can be described as

$$\mathbf{M\ddot{U} + D\dot{U} + KU = F} \tag{1}$$

where $\mathbf{M}$, $\mathbf{D}$, $\mathbf{K}$ are mass, damping, and stiffness matrices of the structure respectively; $\mathbf{U, \ddot{U}}$ are nodal coordinates matrices of the structure; $\mathbf{F}$ are external forces on the structure nodes.

By the centered finite difference form, the nodal velocity can be approximated as

$$\dot{\mathbf{U}}^t = \frac{\dot{\mathbf{U}}^{t+\Delta t/2} - \dot{\mathbf{U}}^{t-\Delta t/2}}{2} \tag{2}$$

the nodal acceleration can be approximated as

$$\ddot{\mathbf{U}}^t = \frac{\dot{\mathbf{U}}^{t+\Delta t/2} - \dot{\mathbf{U}}^{t-\Delta t/2}}{\Delta t} \tag{3}$$

Substituting Eq. (2) and Eq. (3) into Eq. (1) yields

$$\dot{\mathbf{U}}^{t+\Delta t/2} = \dot{\mathbf{U}}^{t-\Delta t/2} \left(\frac{\frac{M}{\Delta t} - \frac{D}{2}}{\frac{M}{\Delta t} + \frac{D}{2}}\right) + \left(\frac{\mathbf{F}^t - \mathbf{KU}^t}{\frac{M}{\Delta t} + \frac{D}{2}}\right) \tag{4}$$

Hence, the nodal coordinate can be expressed as

$$\mathbf{U}^{t+\Delta t} = \mathbf{U}^t + \dot{\mathbf{U}}^{t+\Delta t/2} \Delta t \tag{5}$$

2.2. Simulation model
For a six-strut tensegrity with a center payload, the system has 6 struts, 24 tendons, and a payload. The six struts are divided into three pairs, and the struts in each pair are parallel to each other. The center payload of the system is assumed to be contained by a cubic box which is connected to the tensegrity by 24 tendons. Here, the ANSYS 17.0 LS-DYNA Module is used to simulate the tensegrity structures under different impact conditions. The simulation uses explicit 3-D beam elements (BEAM161) for the struts, tension-only cables (LINK167) for the tendons, and 3-D shell elements (SHELL163) for the payload

(Fig. 1). The properties of the structural members are given in Table 1. The weight of the payload is 0.1276g. Note that the cross-sectional shape of the strut is circular. Due to the size of the center payload, the collision between the strut and payload may occur during the free-falling of the system from a given height to a rigid ground. Thus, each strut is divided into 20 beam elements to get more accurate collision processes.

In addition to the structural properties, motion conditions and gravitational acceleration are also considered as the necessary constants and variables. The outside surfaces of the six-strut tensegrity are divided into two types: closed triangle (TC) and open triangle (TO). A TC has three tendon edges, and a TO has two tendon edges. The TC face ground has the strongest deformation ability due to the structure being most readily compressed in this orientation, thus in this paper, the TC face orientation is considered only. The damping coefficient of the structure is set as 0.01. The gravitational acceleration is set as 9.8 m/s and the coefficient of friction of rigidwall is 0.5.
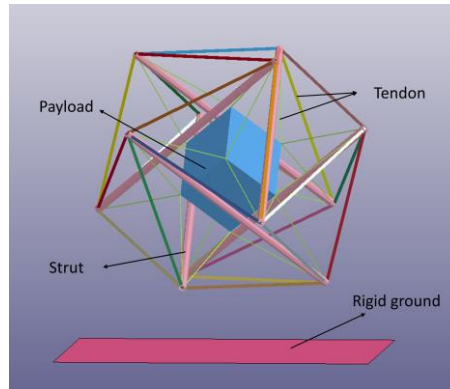

Figure 1: The simulation model of the six-strut tensegrity with a center payload

Table 1: Properties of members

Properties	Strut	Tendon	Payload
Initial Length (m)	0.20	0.06	-
Young's Modulus (GPa)	70	-	2.5
Stiffness (N/m)	-	150	-
Density (kg/m³)	2700	-	3753
Diameter (m)	0.006	0.003	-

To ensure the safety of the system, it is required that all the structural components including the tendons, struts, and the cubic box do not yield or buckle. The failure criteria of the structural components can be defined as four types:

(1) The force of tendons reaches the limit of pulling force. In this paper, the tendons use a type of elastic rope whose maximum draw ratio is 2.3, so the limit of pulling force F_{max}^t can be calculated by

$$F_{max}^t = 2.3 \times L_t \times K_t \tag{6}$$

where L_t and K_t are the initial length and stiffness of tendons respectively.

(2) The struts buckle when their forces reach Euler's critical load. Euler's critical load of struts F_{max}^s can be given by

$$F_{max}^s = \frac{\pi^2 E_s I_s}{L_s^2} \tag{7}$$

where E_s is Young's Modulus of material of struts, I_s and L_s are minimum moment of inertia and length of struts respectively.

(3) The struts yield when their stresses reach yield strength, that is $\sigma_s \le \sigma_{ss}$, where σ_s and σ_{ss} are stress of the strut and yield stress of the material of the strut respectively.

(4) The payload yield when their stresses reach yield strength, that is $\sigma_p \leq \sigma_{sp}$, where σ_p and σ_{sp} are stress of payload and yield stress of the material of the payload respectively.

3. Simulation results

3.1. Dynamic behavior during impact

The simulation of the dynamic behavior of the tensegrity free-falling from a given height to a rigid ground has several key moments. Fig. 2 shows the impact motion of tensegrity when impacting on a TC face with no random rotations during free-falling. After free-falling (Fig. 2a), the structure deforms and begins to compress towards the ground (Fig. 2b). During deformation, the payload contacts the strut (Fig. 2c) and the ground (Fig. 2d). Then the structure begins returning to its equilibrium state (Fig. 2e) and leaves the ground (Fig. 2f).
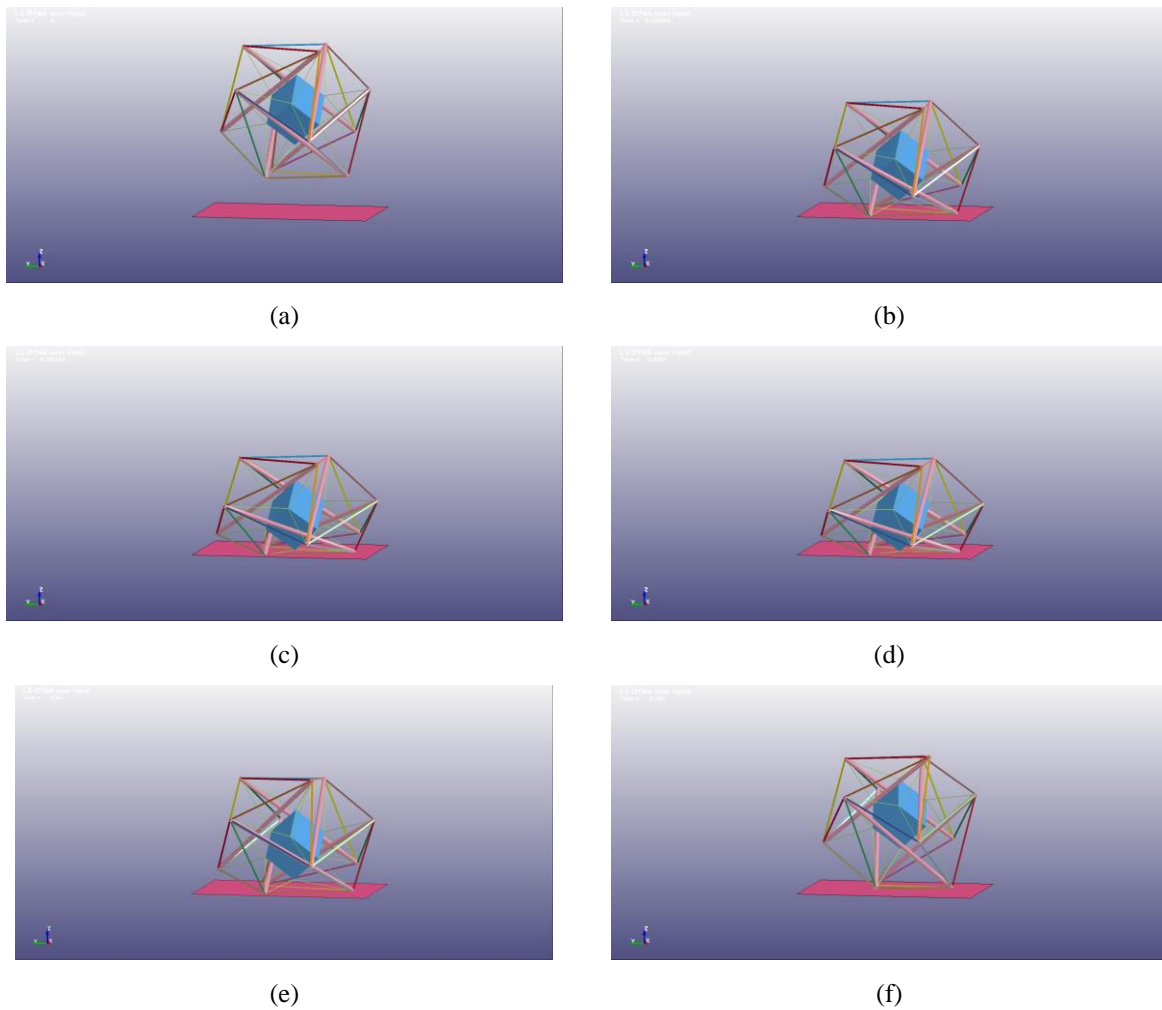

(a)   (b)

(c)   (d)

(e)   (f)

Figure 2: Dynamic behavior of the tensegrity for a 1 m free-falling in simulation model

3.2. Structural parameter analysis

In this section, various structural parameters (stiffness of tendons, prestress, cross-sectional area, length, and material of struts) are examined to assess their influence on the maximum allowable free-falling height achievable by the six-strut tensegrity with a center payload. According to the failure criteria of the structural components mentioned in Section 2, simulation results are shown below.

3.2.1. Stiffness of tendons

In this part, different stiffness of tendons is defined to study the effect on the maximum allowable free-falling height achievable by the system. The prestress of the system, length, cross-sectional area, and material of struts are set as same as those listed in Table 1. As shown in Fig. 3, the maximum allowable free-falling height of the system increases by improving the stiffness of tendons below 600 N/m, and it stay similar when the stiffness of tendons increases above 600 N/m. When the stiffness of tendons is set between 150 N/m and 1200 N/m, the buckling of the struts is the failure form of the structure. It is clear that increasing the stiffness of tendons can improve the impact resistance of tensegrity structure to a certain extent.
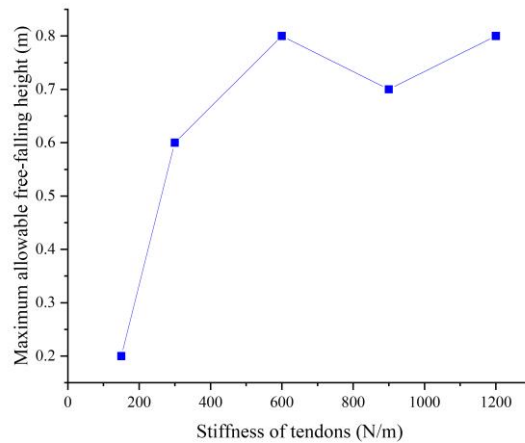

Figure 3: Influence of stiffness of tendons on the maximum allowable free-falling height

3.2.2. Prestress

Here, the influence of prestress in the members on the maximum allowable free-falling height is examined. The stiffness of the tendons is set as 600 N/m, and other properties of members are identical to those listed in Table 1. As shown in Fig. 4, the maximum allowable free-falling height of the system stay equal when the prestress in the members increases below 40.0N. It's worth noting that the buckling of the struts is the failure form of the structure when the prestress is set below 40.0N, but the yielding of tendons becomes the failure form of the structure when the prestress is set as 50.0N, and the maximum allowable free-falling height can't be worked out. That's because the prestress in tendons is too close to the limit of pulling force, the system can't survive after landing. This indicates that the change in prestress of the tendons has little effect on the impact resistance performance of the structure when ensuring its normal operation.
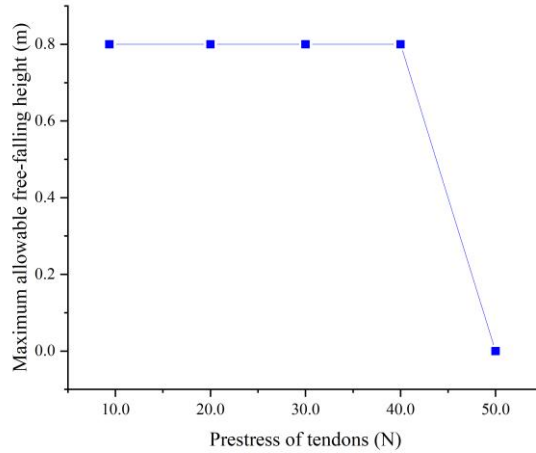
Figure 4: Influence of prestress in tendons on the maximum allowable free-falling height

3.2.3. Cross-sectional area of struts

In this part, to change the cross-sectional area of struts, various diameters of struts are chosen to simulate. The stiffness of the tendons is set as 600 N/m, and other properties of members are set as same as those listed in Table 1. As shown in Fig. 5, it can be seen that the maximum allowable free-falling height of the system decreases when the cross-sectional area of struts increases. When the diameter of struts is 0.006m or 0.008m, the buckling of the struts is the failure form of the structure, and it becomes the yielding of the cubic box when the diameter of struts is 0.010m or 0.012m. This phenomenon can be attributed to the fact that with an increase in the diameter of struts, Euler's critical load of struts increases and the struts buckle more difficultly, but the collision between the struts and the payload is stronger, resulting in the yielding of the cubic box.
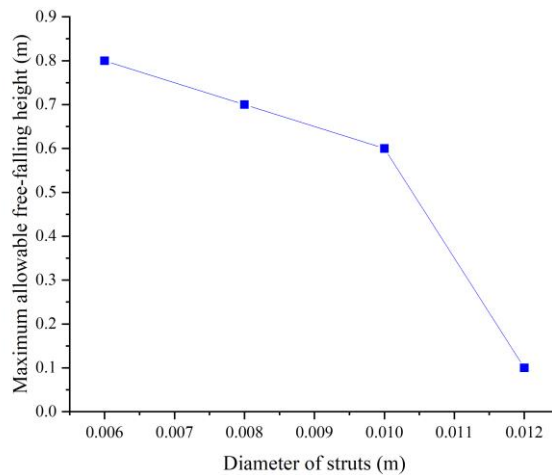

Figure 5: Influence of cross-sectional area of struts on the maximum allowable free-falling height

3.2.4. Length of struts

Different lengths of struts are used to change the size of the tensegrity system. The stiffness of the tendons and the diameter of struts are set as 600 N/m and 0.010m respectively, and other properties of members are identical to those listed in Table 1. As shown in Fig. 6, when the length of struts is defined between 0.2m and 0.5m, the maximum allowable free-falling height of the system decreases by enlarging the size of the tensegrity. When the length of struts is 0.2m, the failure form of structure is the

yielding of the cubic box, and when the length of struts is 0.3m, it becomes the yielding of the cubic box and the buckling of the struts. Besides, when the length of struts becomes more than 0.4m, the failure form of structure is that struts buckle which can be understood easily through Eq. (7). This means that as the length of the struts increases, the collision between the struts and the payload weakens, but the buckling of the struts occurs more easily, resulting in a weaker impact resistance of the structure.
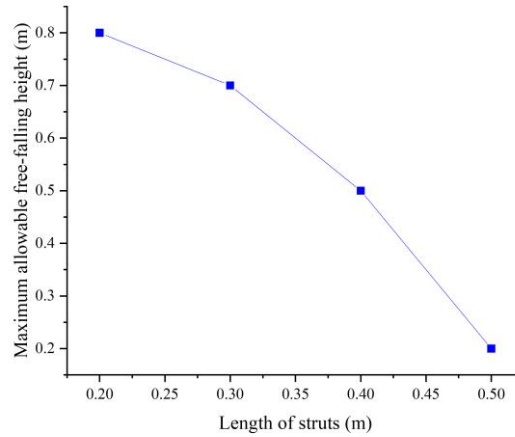

Figure 6: Influence of length of struts on the maximum allowable free-falling height

3.2.5. Material of struts

Since each material has a unique Young's modulus and density, different materials are used for struts. The stiffness of the tendons, the length of struts, and the diameter of struts are set as 600 N/m, 0.4m, and 0.010m, respectively, and other properties of members are identical to those listed in Table 1. The simulation results are listed in Table 6. It is found that material of struts shows a largest influence on maximum allowable free-falling height of the structure comparing to above parameters. In this study, specific modulus, which is defined as elastic modulus per unit density, is introduced to compare the influence of different materials on the maximum allowable free-falling height of the system. As shown in Fig. 7, it can be seen that maximum allowable free-falling height of the structure roughly increases when specific modulus of material increases. Besides, struts with low specific modulus buckle more easily during impact.

Table 2: Influence of material of struts on the maximum allowable free-falling height

| material of struts	Young's modulus (Pa)	Density (kg/m³)	mass of struts (kg)	Limit force of struts (N)	Maximum allowable free-falling height (m)	Failure form of structure
Aluminum alloy	7.00E+10	2700	0.023	2119.57	0.5	struts buckle
Titanium	1.05E+11	4510	0.038	3179.35	0.6	struts buckle
steel	2.07E+11	7800	0.066	6267.87	0.7	struts buckle
UHMWPE	1.20E+11	970	0.008	3633.55	3.0	the cubic box yield and struts buckle
Carbon	2.30E+11	1760	0.015	6964.30	2.6	the cubic box yield
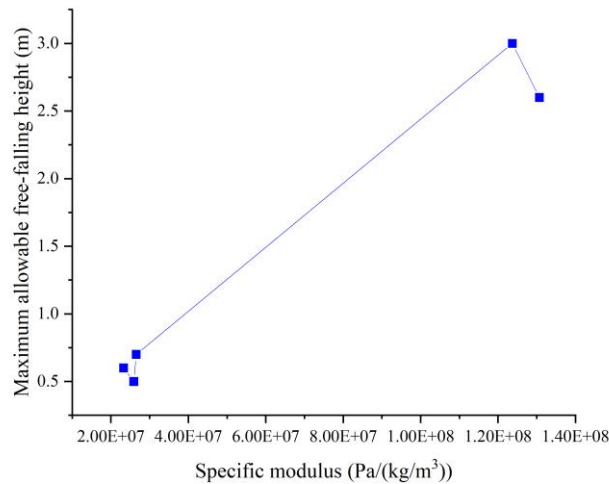
Figure 7: Influence of material of struts on the maximum allowable free-falling height

4. Conclusion

This paper introduces a dynamic model of a six-strut tensegrity system with a center payload and uses the finite element method to simulate the free-falling of the tensegrity from a given height to a rigid ground. The simulation results demonstrate that: (1) Impact resistance of the tensegrity structure is enhanced by choosing struts with high stiffness-to-density ratio and tendons with high stiffness. (2) The failure form of structure can change because of various properties of members. The buckling or yielding of struts or tendons shows a large effect on the impact resistance of the tensegrity structure. Thus, avoiding these failure forms of structure is important during the design of the tensegrity. (3) The change in members' prestress has little influence on the maximum allowable free-falling height of the tensegrity when the structural parameters are certain.

In the future, the physical prototype of the six-strut tensegrity using struts with high stiffness-to-density ratio and tendons with high stiffness can be made to perform drop experiments, so that the accuracy of simulation results can be validated. The material of the center payload can be replaced by TPU or other buffer material to avoid yielding.

References

[1] D.Y.S. Shah, J.W. Booth, R.L. Baines, R.L. Baines, K. Wang, M. Vespignani, K. Bekris and R. Kramer-Bottiglio, "Tensegrity robotics, " *Soft Robot,* vol. 9, no. 4, pp. 639-656, 2021.

[2] S. Ma, M. Chen and R.E Skelton, "Design of a new tensegrity cantilever structure," *Compos Struct,* vol. 243, 112188, 2020.

[3] A. Zhakatayev, B. Abdikadirova, S. Sarmonov and H.A. Varol, "Dynamics of Tensegrity Robots With Negative Stiffness Elements," *Ieee Access,* vol. 8, pp. 187114-187125, 2020.

[4] F. Fraternali, E. De Chiara and R.E. Skelton, "On the use of tensegrity structures for kinetic solar facades of smart buildings," *Smart Mater Struct,* vol. 24, no. 10, 105032, 2015.

[5] A. Zawadzki and A. Al Sabouni-Zawadzka, "In search of lightweight deployable tensegrity columns, " *Appl Sci,* vol. 10, no. 23, 8676, 2020.

[6] J. Rieffel and J.B. Mouret, "Adaptive and resilient soft tensegrity robots, " *Soft Robot,* vol. 5, no.3, pp. 318-329, 2018.

[7] C. Paul, F.J. Valero-Cuevas and H. Lipson, "Design and control of tensegrity robots for locomotion, " *IEEE Trans Robot*, vol. 22, pp. 944–957, 2006.

[8] M. Khazanov, B. Humphreys, W. Keat and J. Rieffel, "Exploiting dynamical complexity in a physical tensegrity robot to achieve locomotion, " in: *Proceedings of the 12th European Conference on Artificial Life, 2013*, pp. 965–972.

[9] A.P. Sabelhaus, J. Bruce, K. Caluwaerts, P. Manovi, R.F. Firoozi, S. Dobi, A.M. Agogino and V. SunSpiral, "System design and locomotion of SUPERball, an untethered tensegrity robot, " in: *Proceedings of the IEEE International Conference on Robotics and Automation, IEEE, Seattle, Washington, 2015*, pp. 2867–2873.

[10] M. Vespignani, J.M. Friesen, V. Sunspiral and J. Bruce, "Design of SUPERball v2, a compliant tensegrity robot for absorbing large impacts, " in: *Proceedings of the IEEE/RSJ International Conference on Intelligent Robots and Systems (IROS), IEEE, Madrid, Spain, 2018*, pp. 2865–2871.

[11] L.H. Chen, K. Kim, E. Tang, K. Li, R. House, E.L. Zhu, K. Fountain, A.M. Agogino, A. Agogino, V. Sunspiral and E. Jung, "Soft Spherical tensegrity robot design using rod-centered actuation and control, " *J. Mech. Robot*, vol. 9, no. 2, 025001, 2017.

[12] K. Kim, D. Moon, J.Y. Bin and A.M. Agogino, "Design of a spherical tensegrity robot for dynamic locomotion, " in: *Proceedings of the IEEE/RSJ International Conference on Intelligent Robots and Systems (IROS), IEEE, Vancouver, BC, Canada, 2017*, pp. 450–455.

[13] Y.F. Zheng, H.Y. Cai, M.J. Wang, J.J. Yao, X. Xu, C.L. Zhou and Y.Z. Luo, "Rolling gaits of a strut-actuated six-strut spherical tensegrity," *Int J Adv Robot Syst,* vol. 17, no. 5, 1729881420960904, 2020.

[14] J.J. Rimoli, "On the impact tolerance of tensegrity-based planetary landers," in: *57th AIAA/ASCE/AHS/ASC Structures, Structural Dynamics, and Materials Conference, 2016*, pp. 1511.

[15] J.J. Rimoli, "A reduced-order model for the dynamic and post-buckling behavior of tensegrity structures, " *Mech Mater*, vol. 116, pp. 146-157, 2018.

[16] A.S. Zhang, "Design of Impact-Resistant Tensegrity Landers, " Ph.D. dissertation, University of California, Berkeley, America, 2022.

[17] X.S. Wang, A. Luo, H.P. Liu, "Design and analysis of a double-helix tensegrity spherical lander," *Mech Res Commun,* vol. 129, 104091, 2023.

Copyright Declaration

Before publication of your paper in the Proceedings of the IASS Annual Symposium 2024, the Editors and the IASS Secretariat must receive a signed Copyright Declaration. The completed and signed declaration may be uploaded to the EasyChair submission platform or sent as an e-mail attachment to the symposium secretariat (papers@iass2024.org). A scan into a .pdf file of the signed declaration is acceptable in lieu of the signed original. In the case of a contribution by multiple authors, either the corresponding author or an author who has the authority to represent all the other authors should provide his or her address, phone and E-mail and sign the declaration.

Paper Title: _____ Impact resistance of six-strut tensegrity _____

Author(s): _____ Zhaojun Liu, Xian Xu, Meijia Wang, Ruhe Mei _____

Affiliation(s): _ College of Civil Engineering and Architecture, Zhejiang University _

Address: _____ 866 Yuhangtang Road, Hangzhou, Zhejiang 310058, China _____

Phone: _____ 057187952349 _____

E-mail: _____ xianxu@zju.edu.cn _____

I hereby license the International Association for Shell and Spatial Structures to publish this work and to use it for all current and future print and electronic issues of the Proceedings of the IASS Annual Symposia. I understand this licence does not restrict any of the authors' future use or reproduction of the contents of this work. I also understand that the first-page footer of the manuscript is to bear the appropriately completed notation:

If the contribution contains materials bearing a copyright by others, I further affirm that (1) the authors have secured and retained formal permission to reproduce such materials, and (2) any and all such materials are properly acknowledged by reference citations and/or with credits in the captions of photos/figures/tables.

Printed name: Xian Xu

Signature: _____
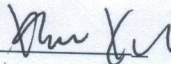
Location: Hang Zhou

Date: _____ 01-07-2024 _____